# Mechanisms of failure on terraced slopes: the Valtellina case (northern Italy)

Corrado A. S. Camera*✉, Tiziana Apuani*, and Marco Masetti*

**Università degli Studi di Milano – Dipartimento di Scienze della Terra A. Desio*

✉ corresponding author

Phone: +39 02 503.155 01

Fax: +39 02 503.15494

*Email: corrado.camera@unimi.it, c.camera@cyi.ac.cy*

# ABSTRACT

Slopes that are terraced by means of dry-stone retaining walls are very common in the alpine environment. In Valtellina, a typical Italian alpine valley, these slopes are widespread and quite often involved in superficial mass movements that can result in severe damage and casualties. For an in-depth understanding of the processes that can trigger these events, numerical modeling of groundwater movement and a related stability analysis were performed on a detailed scale, based on an intensive monitoring of rainfall events and groundwater movement. Field observations suggest that the formation of a perched groundwater table at the contact between the bedrock and the backfill soil of walls as well as the concomitant saturation of this backfill soil are the determining factors of potential slope failure. The numerical models support these observations. In addition, the models are able to explain the mechanisms of formation of perched water tables, highlighting the factors that can influence groundwater levels and slope instabilities.

*Keywords: dry-stone walls, failure mechanisms, unsaturated-saturated soils, numerical modeling, Valtellina*

# INTRODUCTION

In May 1983, July 1987, and November 2000, Valtellina valley, in Northern Italy (Fig. 1), experienced prolonged periods of intense rainfall that produced widespread landslides along the whole valley (Cancelli and Nova 1985, Guzzetti et al. 1992, Crosta et al. 2003). According to Crosta (1990) and Crosta et al. (2003), more than 200 superficial landslides affected Valtellina in 1983. In 1987, the huge Val Pola landslide (40 million $m^3$), which was a landslide that claimed 12 victims, was the largest of a series of hundreds of mass movements that occurred throughout the entire valley from Dubino to Bormio (Fig. 1). In November 2000, 260 shallow landslides were observed in only four days in the lower-middle part of the valley between Dubino and Tirano.

In all three cases, the worst affected areas were the slopes that were terraced by means of dry-stone walls on the northern flank of the valley between Sondrio and

Tirano (Cancelli and Nova 1985; Crosta et al. 2003). These movements often originate from soil slips or shallow landslides after a Coulomb-type failure and then evolve into potentially destructive avalanche influenced by the increase of pore water pressure (Fleming et al. 1989; Iverson et al. 1997; Johnson and Rahn 1970).

It is therefore clear that a stability analysis of the terraced slopes in Valtellina is a key issue to assess and improve infrastructure safety and potentially save lives. The final aim is to construct an instrument capable of predicting the timing and location of rapid shallow landslides on terraced slopes induced by rainfall.

Apip et al. (2010) summarized three different approaches to the problem that have been used during the last years. The first approach regards the determination of rainfall thresholds that can trigger superficial landslide events in some areas, both at site-specific and regional scales (Caine 1980; Ceriani et al. 1992; Crozier 1999; Bacchini and Zannoni 2003; Zezere et al. 2005; Jacob et al. 2006; Guzzetti et al. 2008). The second approach consists of statistical methods in which rainfall is recognized as the triggering factor in mass movement events and can be used as an explanatory (independent) variable in the analysis (Lee and Pradhan 2007; Dahal et al. 2008; Choi et al. 2010; Pradhan and Lee 2010). The third approach consists of physical-based modeling of the hydrologic processes, where rainfall is the most important input variable in the analysis of its relationship with stability (van Beek and van Asch 2004; Salciarini et al. 2006; Simoni et al. 2008; Kuriakose et al. 2009; Montrasio et al. 2009). Such an analysis, conducted on a catchment scale, should reveal the areas that are prone to trigger superficial landslides. The present work is intended to follow this third approach; however, considering the particular morphology of the area and the central role that dry-stone walls are expected to play, a detailed analysis on the single terrace scale was conducted before expanding the scope of study to the entire small catchment. This decision was made to first improve our knowledge of the hydrogeological and mechanical properties associated with dry-stone walls and how these walls affect groundwater flow in the slope.

Previous authors have studied the strength of dry-stone wall structures through numerical modeling (Harkness et al. 2000; Powrie et al. 2002; Zhang et al. 2004; Walker et al. 2007), through analytical models (Villemus et al. 2007) or by combining these two approaches (Lourenço et al. 2005). However, studies where dry-stone walls have been considered directly in slope stability analysis have proven difficult to find. Crosta et al. (2003) highlighted the lack of maintenance of dry-stone retaining walls as a possible contributing factor in slope failure in the same geomorphological context. However, this study was in a stratigraphic setting where an upper horizon of human-worked, permeable soil rested on a more compacted layer that acted as a hydrological barrier, and this work did not deal directly with the physical characteristics of the dry-stone walls themselves.

The aim of the present work is to analyze the processes that can lead to failure, both from a qualitative and quantitative perspective, referring to field observations and results from monitoring activity, and by making use of numerical modeling. In an earlier work (Camera et al. 2012), the relationships between rainfall events and the formation of perched groundwater tables (hereafter referred to as PGTs) were analyzed, and it was possible to set up a hydrogeological model capable of reproducing the dynamics of water table formation on the terrace scale. The hydrogeological model can be used to provide pore water pressure distributions, which are generated by different rainfall amounts, as parameters for a stress-strain analysis that can directly determine the influence of various rainfall parameters on dry-stone wall stability. These parameters include rainfall intensity and duration and, more importantly, the antecedent moisture content related to the rainfall (Corominas and Moya 1999; Rahardjo et al. 2001; Jakob and Lambert 2009; Khan et al. 2011) and the rainfall patterns (Ibsen and Casagli 2004; Tsai 2008) that preceded the event of interest. The proposed procedure enables the quantification of hydrogeological and mechanical characteristics of the walls and the distinction between well maintained and poorly maintained structures. This investigation focuses on the main causes of failure among the triggering factors that are related to the formation of PGTs in the backfill of dry-stone walls with rainfall as the primary input; it does not consider aspects related to directional drainage as a contributing factor. However, this contributing factor should not change either the mechanisms of failure or the critical water table levels and would not affect the relative importance of the factors analyzed in this work.

# STUDY AREA

Valtellina is a glacial valley in the Central Alps of northern Italy (Fig. 1). It is superimposed on a regional fault, the Periadriatic Line, which divides the alpine chain *sensu stricto,* from the southern alpine units. In particular, in the area of interest, the Tonale regional lineament separates the Austroalpine Metamorphic Basement (Alpine age) represented by Languard-Tonale Tectonometamorphic Unit (LTB, LTN and LTX in Fig. 2) with the Aprica Tectonometamorphic Unit (APX and APQ in Fig. 2) belonging to the Variscan Metamorphic Basement of the Southern Alps (Gosso et al. in press). The principal trend of the valley is E-W from Dubino to Tirano becoming NE-SW in its upper part to Bormio. The valley floor, where the Adda River flows before joining the Como Lake near Dubino, is up to 3 km wide. For the northern terraced flank of the valley, Crosta et al. (2003) recognize an average slope gradient (driven by the bedrock geometry) of 42°, while the gradient along a single terrace is typically comprises between 15° and 25° with extreme cases above 40°. The slopes are covered with soils of glacial and colluvial origin that, considering the high relief of the area, are prone to trigger soil slips and debris flows both on open slopes and in channels.

Figure 1: Geographical setting of the study area.

Figure 2: simplified geological map of the study area and surrounding area (modified after Gosso et al, in press) Neogene to Quaternary continental deposits: **POI** = Po Syntheme; **LCN** = Cantù Syntheme; Austroalpine metamorphic basement - Languard-Tonale tectonometamorphic unit: **LTB** = two mica- or biotite- metasedimentary gneisses; **LTN** = sillimanite, biotite and garnet metasedimentary gneisses; **LTX** = garnet – staurolite micaschists; Variscan metamorphic basement of the southern Alps - Aprica tectonometamorphic units: **APX** = garnet, biotite and chlorite micaschists, **APQ** = Quartzites.

Terraced slopes for vineyard cultivation are present on the northern flank in the central part of the valley, covering a surface of 17 $km^2$ (Crosta et al. 2003). One of these areas is the slope uphill of the village of Tresenda. Tresenda was chosen as a study area because it possesses representative characteristics of Valtellina terraced slopes and also because it was investigated in 1983 and 2002 for soil slip/debris avalanche (Hungr et al. 2001, 2012) events (Fig. 3) that caused damage to vineyards, buildings, roads, and other infrastructure and resulted in human casualties (Azzola and Tuia 1983; Cancelli and Nova 1985; Quan Luna et al. 2010; Blahut et al. 2012; Camera et al. 2012).

Figure 3: two photos of the soil slip/debris avalanche events that in May 1983 affected the slope of Tresenda. Top: a panoramic of the slope; bottom: a detail of the source area of the event on the left in the top image. Photos by Maurizio Azzola.

A morphological natural terrace, along with trenches and counterslopes present in the upper part of the slope, highlights a condition of general instability that is partially controlled by the presence of man made terraces and dry-stone walls. Most of the walls are between 1.4 and 2.5 m high, while terrace length and width depend on slope morphological characteristics (slope angle, soil depth and number of bedrock outcrops), but in general they are between 20-100 m long and 5-25 m wide. Few outcrops of rock masses are present in the area (Fig. 2). The bedrock is constituted by a fine grained schist (APX) with white mica, garnet, plagioclase, quartz, ± biotite, ±chlorite, also known as Edolo Schists (Beltrami et al. 1971), interlayed by quartzites (APQ), commonly foliated pinkish gray rocks, with white mica and chlorite, and are locally interrupted by lens of epidotic amphibolites. When outcropping, the rock mass appears irregular, with four principal discontinuity sets. The first one is more or less parallel to the schistosity planes with dip direction towards N, so towards upslope, and high dip. The second set has a dip direction towards S-SE and a mean dip of 45°. The third set presents a similar mean dip while the dip direction is oriented SW. The last set of discontinuities shows a dip direction towards E-NE and a mean dip of 60°. All these discontinuities are joints and except for rare occasions they are closed, so the schists are a low hydraulic conductivity formation acting as an aquiclude at the base of the surficial permeable soils. Uphill, out of the area of study, the metasedimentary gneiss (two mica- or biotite- gneisses LTB and sillimanite, biotite and garnet gneisses LTN) of the Languard-Tonale Tectonometamorphic Unit (Alpine Age) overlaps the Variscan units. The soils that are not of glacial and colluvial origin are mainly constituted by filling material, especially on the terraces. Other important characteristics of the study area include the presence of paved roads for accessing to the vineyards, which can act as superficial drainage channels that break up the hydrogeological continuity of the slope during episodes of intense rainfall (Revellino et al. 2008), and a drainage system made up of smaller channels that permit excess water runoff.

# RAINFALL EVENTS AND PERCHED GROUNDWATER TABLES

Various instruments were installed and field tests were performed during the summer of 2009. In particular, seven piezometers, two equipped with a data logger for continuous acquisition, and two manual tensiometers were installed. The aim was to register events of PGTs formation in the shallow soil present at the top of the bedrock, where no permanent groundwater tables are present.

All piezometers reached a depth around 100 cm, except for one located in the lower part of the slope which arrives at 140 cm under the terrain surface. The data collectors used during the work are Keller's DCX-22 AA, which measure water levels using a two sensors technology. A submersible depth sensor measures the water level while a sensor in the electronic component of the instrument at the top of the borehole measures barometric pressure variations so that the measures are compensated. One of the data loggers was installed in a piezometer in the upper part of the slope and kept there for the entire duration of the monitoring activity. The piezometer was located in the upper part of a terrace, around 2.5 m downhill of the dry stone wall of its uphill terrace. The second data logger was moved during the monitoring period in different sites in the lower-middle part of the slope to investigate the response of water table in different areas and in different locations with respect to the piezometer position along a terrace. For a more complete description of field tests, their location, and monitoring activity in general see Camera et al. (2012).

As of August 2011, 133 precipitation events were registered based on the criterion that a discrete rainfall event ends when the last hour of rainfall is followed by at least 12 hours without rain. A PGT will form after 24 such events. Comparison of the data registered by the piezometers with actual rainfall events permits the correlation between some characteristics of the precipitation events and changes in the PGTs. Most notably, rising PGT correlates more directly to rainfall intensity whereas PGT spatial and/or temporal persistence seems to depend more on the duration of rainfall after its peak (Camera et al. 2012). The same data are presented in the form of an intensity-duration rainfall threshold for PGT formation (Fig. 4a), which is modeled after previous examples that were correlated to landslide triggering in Valtellina (Cancelli and Nova 1985; Govi et al. 1985; Ceriani et al. 1992; Agostoni et al. 1997; Crosta and Frattini 2001; Luino et al. 2008). This threshold was drawn using the data recorded between August 2009 and 2010, and it was then validated with data from 2011 (Fig. 4b). The aim was to monitor the formation of perched groundwater tables and the trend of water content in the soil in relation to rainfall events recorded on an hourly basis by a meteorological station (Castelvetro/Somasassa) located 300 m north of study area. It is important to note that the threshold in Fig. 4 is only a first and rough estimate of the potential to observe slope instability as it relates to rainfall and PGT; it does not address any probability of collapse that is related to water table levels and critical states of stress.

To provide a broader context for rainfall characteristics on a larger temporal scale, a statistical analysis was performed for precipitation data spanning 27 years (1980-2002 and 2007-2010) from the nearby rain station of Castelvetro/Somasassa, and intensity-duration curves for different return periods (Fig. 5) were determined (Quan Luna et al. 2010; Camera et al. 2012) based on this analysis.

Figure 4: Rainfall intensity-duration threshold for perched groundwater table (PGT) formation. a) The threshold drawn from the data of the period August 2009 - August 2010 as presented in Camera et al. (2012); b) validation of the threshold performed with the data from August 2010 – August 2011.

Figure 5: Rainfall intensity-duration frequency curves for return periods (T) of 10, 25, 50, and 100 years. The three points on the graph depict the landslide triggering rainfall event of 1983 by associating the recurrence time to three pairs of cumulated duration-height recorded before the triggering of the three debris avalanches occurred on the 22$^{nd}$ and 23$^{rd}$ May 1983.

# FIELD TESTS AND LABORATORY ANALYSIS

Three types of tests were performed in the field (Table 1) for a first characterization of backfill soils: double ring infiltrometric tests (DR), hole infiltrometric tests (H), and soil density measurements with the sand cone method (ASTM 2007). Samples were also collected to perform laboratory analysis for a further hydrogeological and geotechnical parameterization of the soils. Granulometric analysis (ASTM 2010), falling (FH) and constant head (CH) permeability tests (ASTM 2006), and direct shear tests to determine the peak and residual soil strength according to ASTM 2004 were carried out on remolded samples, most of them collected in the sites where the piezometers had been previously installed, but with a particular attention in having samples from the different land use recognized in the area. All of the mean values of parameters with their range of variation are summarized in Table 1. According to the Unified Soil Classification System (U.S.C.S), the investigated soils are SM (silty sand with gravel) or GM (silty gravel with sand).

Table 1: Summary of the hydrogeological and geotechnical principal properties of the backfill soils: saturated hydraulic conductivity ($k_s$); dry and natural bulk weight ($\gamma_d$ and $\gamma_0$ respectively); peak values of cohesion ($c_p$) and friction angle ($\phi_p$).

# INFILTRATION AND GROUNDWATER MODELING

Analysis of groundwater flow has been described in detail in Camera et al. (2012). Here, only a brief summary of their main results is given to better support the approach and results obtained in the following stability analysis. The slope conceptual model consists of a series of terraces where the dry-stone walls are founded on bedrock (or on a competent layer of soil) and on which there is a layer of permeable backfill soil set up by glacial, fluvio-glacial and moraine sediments, all modified by human activity. For the numerical modeling analysis, a simple one-terrace geometry has been depicted graphically (Fig. 6). Wall heights, the slope angle of the bedrock-soil contact, and surface topography were derived both from field data and from data provided in Cancelli and Nova (1985) and Crosta et al. (2003).

Figure 6: Model geometry and boundary conditions.

SEEP/W (GEOSLOPE International Ltd. 2002a), which is a finite elements code that can account for both saturated and unsaturated soil conditions, was used for numerical simulation of infiltration and groundwater movement processes. The required input for characterizing the different materials involved are the saturated hydraulic conductivity ($k_s$), the soil water retention curve (SWRC), and the permeability function. Input data were derived from field and laboratory tests and adjusted during the calibration phase of the model. The model was calibrated and validated using two different rainfall events registered by the meteorological station and by comparing the hydrographs – PGT levels vs. time – registered by the piezometer data logger installed for this study with the hydrographs calculated by the model.

To better understand the processes that lead to the formation of PGTs in these contexts, a sensitivity analysis was also performed. Increases in wall height and lowering of bedrock slope angle cause a higher maximum water table level, while increases of both isotropic and anisotropic $k_s$ cause decreases in water levels. In addition, the saturated horizon is lengthened in correlation to the ratio between vertical and horizontal $k_s$ and bedrock slope angle. All of the considered variables have some influence on the dynamic of formation and development of PGTs, underscoring the complexity of the process. In particular, when rainfall intensity is sufficiently high, a water table begins to form in the upper part of the terrace where the low hydraulic conductivity bedrock is close to the topographic surface. As soon as the water table forms, the groundwater flows downhill along the soil–bedrock interface, where it can also be fed by infiltration in the lower part of the slope.

The possibility that a significant water table reaches the back of the wall mainly depends on the combination of soil hydraulic characteristics and geometry coupled with rainfall intensity and duration. If the nearly formed water table in the upper part of the slope is not adequately fed for a sufficient time in its movement downhill, then it spreads throughout the soil without forming a saturated zone in the lower part of the slope.

Finally, the model was applied with a synthetic project rainfall lasting 72 hours and characterized by constant intensity, obtained from statistical elaboration (Quan Luna et al. 2010; Camera et al. 2012), similar to the one which caused the triggering of the shallow landslide in May 1983. Two different limit conditions were considered, on the base of wall status in the area: well maintained wall, where the initial draining condition of the wall was still active and poorly maintained wall, where clogging between stones had occurred. The first situation was modeled considering the wall with a high hydraulic conductivity (1E-4 m/s) while the second with a low hydraulic conductivity (1E-6 m/s) It is interesting to see how the overpressure developed at base of the wall varies for different conditions of maintenance of the walls (Fig. 7).

Figure 7: Overpressures developed at the wall base (kPa) for the project rainfall event of 72 hours and 50 years return period, with a well-maintained wall (a) and an old, poorly maintained structure (b). Results obtained from SEEP/W.

# STABILITY ANALYSIS

## Finite Elements Stress-Strain Analysis

SIGMA/W (GEOSLOPE International Ltd., 2002b) was used to compute the stability of the system. It calculates the stress and strain field that corresponds to different pore water pressure conditions derived from previous SEEP/W analyses. The geometry of the system is the same as Fig. 6. The strength parameters of the soil were derived from laboratory direct shear tests, considering a cohesion equal to 10 kPa and a friction angle of 30°. A cohesion of 345 kPa and a friction angle of 40° were assigned to bedrock. These parameters are set relatively high to ensure that the bedrock behaves as a rigid material to avoid any influence it may exert in the interaction between the soil and the wall.

The mechanical parameterization of the dry-stone wall was more complicated. The dry-stone wall is a particular structure made up of stones fitted together with exacting techniques that exclude the use of cement or grout (Fig. 8).

Figure 8: A dry-stone wall with the stones and voids structure.

Mechanical parameters were determined through back analysis using as an input the pore pressure distributions calculated by the groundwater model from three similar past rainfall events (May 1981, May 1983 and November 2009), one of which produced instability (1983). Using the same dry initial condition with which the groundwater model was calibrated, it was not possible to distinguish the individual effects of the three discrete rainfall events that had a similar duration (64 hours in 1981; 66 hours in 1983 and 76 in 2009); at least two of them had a similar total cumulative rainfall (178 mm in 1981, 176 mm in 1983 and 76 in 2009). However, when considering the 15 previous days of antecedent precipitation (51 mm, 163 mm, and 2 mm in 1981, 1983, and 2009, respectively), the unstable event (of 1983) can be correctly identified and reproduced in terms of time of collapse in relation to the initiation of the critical rainfall event.

### *Model Preliminary Results*

The wall parameters reproducing the three above mentioned conditions resulted in a cohesion of 120 kPa, a friction angle of 55°, an elastic modulus of $2.5 \times 10^5$ kPa and a Poisson's ratio of 0.32. SIGMA/W also considered the evolution of the matric potential in the unsaturated zone, as calculated by SEEP/W, through the $phi_b$ parameter, which is related to apparent cohesion. The failure criterion adopted here is the Fredlund-Rahardjo criterion (Fredlund and Rahardjo 1993), which is a modification of the more familiar Mohr-Coulomb criterion.

The two stable cases that were examined during the calibration phase show that stability is affected not only by the values of cohesion and the friction angle of the wall but also by the elastic modulus. There is a narrow optimum window for this value, above which the wall is too rigid to adapt itself to soil pressures and below which it is too soft to resist the same pressures.

The pore water pressure distribution at collapse, obtained by simulating the May 1983 event (Fig. 9), is consistent with the description of Azzola and Tuia (1983), who observed saturated backfill soils during the triggering of the second superficial landslide. However, the main problem shown by the model is that it is unable to correctly reproduce the mechanism of failure observed on site. Azzola and Tuia (1983) described saturation of the backfill soil, followed by a bulging at the toe of the dry-stone wall and then by subsequent collapse of both the wall and soil. Figure 9 shows how this mechanism can be overlooked. As predicted, the positive shear strain is concentrated at the base of the wall (Fig. 9b); however, most likely for numerical reasons, the model balances this strain with an uphill displacement of the middle to lower part of the wall rather than a homogeneous downhill movement. Such a numerical solution could be affected by the variability in rigidity between the wall and the bedrock to which it is bound, and perhaps also by algorithm artifacts that do not take into account large strains that allow the grid to be updated after each calculation step.

Figure 9: a) Time of failure represented by the displacements experienced by the wall; b) XY shear strain [-] developed in the model. Results obtained from SIGMA/W.

## Stress-Strain Finite Differences Analysis

To better reproduce the actual mechanism of the dry-stone wall failure, a finite differences (FD) numerical analysis using the FLAC 6.0 code (Fast Lagrangian Analysis of Continua - Itasca Consulting Group Inc. 2008) was performed. General results of the two different codes were also compared to determine if they were consistent with each other, thus confirming their reliability. The same geometry was reconstructed and the grid was reproduced as closely as possible to the one of SEEP/W and SIGMA/W. The main difference between the two programs is that the FLAC separates the wall from the soil and bedrock by means of interfaces to treat forces and pressures independently, without being linked to the rest of the system. Another difference is related to the failure criterion, as the FLAC simulation does not allow considering the contribution of apparent cohesion ($phi_b$) of the unsaturated soils. Mechanical and hydrogeological properties were assigned to the materials with the calibrated values obtained from the previous modeling phases, and with an initialization of the state of stress achieved by cycling the model in dry conditions until an elastic equilibrium state was reached. As the infiltration and groundwater movement process was well simulated by SEEP/W, it was decided that the groundwater table geometry could be reproduced by applying a constant infiltration on the terrain surface, cycling the model only for groundwater flow purposes, until the pore water pressure distribution matched that which was obtained by groundwater numerical modeling.

### *Model preliminary results*

The most critical water table levels for the three analyzed rainfall events, as calculated by SEEP/W, were reproduced both for a draining and non-draining wall. Concerning the mechanical analysis, the physical parameters of the wall calibrated with SIGMA/W appeared to be too high, mostly in terms of cohesion, because the system always remains stable. Instability is observed for the 1983 event with a non-draining wall, lowering the wall cohesion value from 120 kPa to 15 kPa.

Additionally, a sensitivity analysis was performed on the properties of the soil-wall (sw) interface and on the wall-bedrock (wb) interface. The sw-interface was treated as an unbonded contact, so movement along it was always possible. In contrast, the wb-interface was considered to be rigidly bonded, with movement along this contact possible only when a certain stress threshold was exceeded. Along both interfaces cohesion was set to zero, so the parameters analyzed were the friction angles and the threshold strength of the bonded wb-interface. By changing these parameters, FLAC is able to reproduce different mechanisms of failure. Considering rigid interfaces, i.e., those with high friction angles and/or a highly elevated value of the threshold strength of the wb interface, the predominant mechanism for wall failure is toppling both in the early and in the final stages of collapse. In this case, the friction angle between the wall and the bedrock (and more generally, the bonded behavior of the wb-interface) does not allow the wall to slide at the base; the deformation zone does not include the base of the wall (Fig. 10a,b). By lowering the friction angle and threshold strength at the contact between wall and bedrock, the simulation appears to better reproduce the mechanism of failure as observed on site in 1983 (Fig. 10c,d). It is possible in this simulation to observe an initial toppling (Fig. 10c) that later evolves into bulging and sliding at the base of the wall (Fig. 10d) until collapse occurs.

In general, the higher the friction angles of interfaces, the more evident the toppling mechanism becomes. On the other extreme, if the wb-interface friction angle becomes too low (< 20°), the wall tends to dilate, the entire structure expands, and a clear collapse mechanism is not discernible. Regarding the threshold strength, optima are between 25 and 40 kPa. Higher values show a little movement at the base of the wall, but the system reaches equilibrium without collapsing.

Figure 10: Results obtained from FLAC showing the shear strain increments and the displacement vectors. Initial (a,c) and final (b,d) failure mechanisms depending from soil-wall (sw) and wall-bedrock (wb) friction angle.

## Results and discussion

Once calibrated and validated, the models were run using the outputs of the groundwater model obtained for the project, with statistical rainfall inputs of constant intensity, duration of 72 hours (similar to the one that caused instability), and return period of 10, 50, and 100 years. Each input considered, as an additional variable, the different state of maintenance of the wall under both dry and wet conditions, the latter of which being similar to the conditions produced by the 15 days of precipitation prior to the event that led to instability. Changing only the cohesion value, the results obtained with SIGMA/W can be replicated by FLAC (Table 2), with the exception of simulations 8 and 10 that, with FLAC, resulted in collapse and instability, respectively.

Table 2: Summary of the results obtained using the calibrated stability model. During the different simulations, the return period of input rainfalls, wall maintenance conditions, and initial volumetric water content of the soil were varied.

The first noteworthy result is that both models are consistent in the calculation of stability for dry initial conditions with every rainfall return period and with both well maintained and poorly maintained walls. In addition, both models reproduce a failure for the worst scenario (Table 2, simulation 12). Thus, the triggering of superficial landslides should occur only with a combination of an extreme rainfall event following an extended period of rainfall.

Conversely, the two models are not in agreement in the case of simulations 8 and 10. Simulation 8 considered a 50-year return period of rainfall, a poorly maintained wall, and nearly saturated soil at the beginning of the critical rainfall event. The FD model predicts instability for this simulation, which is consistent with its calibration. In fact, the unstable rainfall event (May 1983) used during the calibration phase has a return period of less than 50 years (Fig 5). Regarding the FE analysis, the observed stability in this circumstance can indicate that the pattern of rainfall distribution within the same event can influence the process analyzed. Statistically generated rainfall projections are applied as episodes of constant rainfall intensity. The differences between the two models become even more significant with consideration that the FD model does not consider the evolution of matric suction. Unsaturated soil is not considered in this type of analysis; the soil is always saturated, and the formation of a perched water table is exacerbated by water pressures. In this context, failure occurs once a threshold water level is reached. Higher rainfall input corresponds to a higher maximum water level, and consequently, failure is certain. By contrast, the FE analysis considers the unsaturated horizon from both a hydrogeological and geotechnical perspective, generating one more variable that is represented by the relationship between the saturated and unsaturated soil. Considering the higher cohesion value of the wall, as incorporated into the FE model, it is possible to hypothesize that a weakness zone, due to the dissipation of matric suction, can develop at the contact between the saturated and the unsaturated soil (Tsai et al. 2008). A further proof of the probable existence of a zone of weakness at the contact between the saturated and unsaturated soil derives from the instability returned by the FE model at the end of simulation 10. This collapse is particularly interesting because it occurred with a very high rainfall return period with a well-maintained wall. This result is unexpected, even when considering the previous literature (Azzola and Tuia 1983; Cancelli and Nova 1985; Crosta et al. 2003). In fact, differences are noticeable when comparing the failure mechanisms of simulations 10 and 12 for the FE model (Fig. 11) referring to a well maintained and poorly maintained wall condition respectively. In case of a well maintained wall (simulation 10, Fig

11a, b), there was no zone with high positive pore water pressure at the base of the wall (Fig. 11a); the failure surface develops within the soil, involving all of its height (Fig. 11b). The failure surface seems in part to resemble the contact between saturated and unsaturated soil, thus indicating that the failure is determined by a matric suction dissipation. The possibility of failure related to this cause is clarified by some failures registered during the calibration phase of the FE model (Fig. 12). In the reported images, the pore water pressure distribution is correlated to the maximum shear stress, which approximately develops at the contact between the saturated and the unsaturated soil or where there is a high matric suction gradient. The failure for a poorly maintained wall (simulation 12, Fig. 11c, d) was driven by an increase of the pressure on the wall due to a rise of the water table. Pore water pressure was maximum at its base (Fig. 11c), and the concentration of stress and strain in that position led to a failure at the contact between the soil or wall on one side and bedrock on the other (Fig. 11d). Of the two failure mechanisms described above, the last one, due to the formation of high positive pore water pressures at the base of the wall, was that observed on-site in 1983 and reported by Azzola and Tuia (1983). This mechanism seems to be more probable than the other one, considering that, for particular patterns of rainfall distribution, it is possible for events with a return period between 25 and 50 years (e.g., the event of 1983). The possibility of a failure triggered by the first mechanism (matric suction dissipation) is predicted by the FE model only in response to a rainfall event with a 100 year return period, but no field descriptions of this mechanism are available. The existence of this mechanism must be acknowledged, but the more significant mechanisms are related to the formation of high positive pore water pressures. Therefore, proper maintenance of the walls might reduce the hazard related to superficial landslides in the analyzed morphological context, but it cannot eliminate the hazard altogether.

Figure 11: Pore water pressure distribution in kPa at the moment of collapse for a well maintained wall (a) and a poorly maintained wall (c) as calculated from SEEP/W. b) and d): The corresponding states of XY shear strain, showing different failure surfaces as calculated from SIGMA/W.

Figure 12: Contours represent the pore pressure distribution at the time step immediately prior to the collapse for three different combinations of cohesion and friction angle values for the wall. The simulations refer to the calibration phase performed with the FE model. a) $c = 30$ kPa, $\phi = 50°$; b) $c = 40$ kPa, $\phi = 50°$; c) $c = 90$ kPa, $\phi = 55°$. The contour of the maximum shear stress tends to develop at the contact between the saturated and unsaturated soil.

# CONCLUSION

Stability analysis and hillslope hydrology are closely connected when studying the causes for triggering shallow landslides in mountainous areas. On a terraced slope, these dynamics are further complicated by the presence of retaining walls, which introduce other variables in the process.

Based on the conceptual model of the study area, a first approach was to study the relationship between the rainfall events and the PGTs that can form in the backfill soils behind the walls because these are considered to be the main possible cause of instability. An intensity-duration threshold for the onset of a PGT, which can be considered as a first indication of danger for real-time applications, was derived and validated. It was also determined that the water table formation is correlated to the intensity of the rainfall event more than any other single factor, whereas the exhaustion time depends more on the amount of rain that falls in the final part of the event.

Next, a groundwater finite elements model representing a single terrace was constructed to further understand the dynamics of formation of PGTs. The results demonstrate that both isotropic and anisotropic hydraulic conductivity of soil highly influence the outcomes, which are also affected by changes in bedrock slope and wall height. The model is also able to quantify the difference in the behavior of a well maintained wall as opposed to a poorly maintained wall. This difference is simulated by changing the values of hydraulic conductivity assigned to the wall.

Finally, a stability analysis was performed through two different numerical modeling codes. A finite differences analysis was added to the FE analysis that was also performed for the groundwater flow study. To include all the processes in the analysis that contribute to the formation of PGTs, the computed piezometric levels from the calibrated groundwater model, corresponding to different rainfall events, were used as input data. Comparison of the results obtained with the FE and the FD codes permitted the calibration of the mechanical properties of the dry retaining walls while simultaneously analyzing the effects on slope stability of various factors, including initial moisture content conditions, return periods of the rainfall events, maintenance characteristics of walls, and rainfall patterns. Critical water table levels can be reached only by the combination of an extreme rainfall event of relatively short duration (72 hours) and an antecedent extended rainfall. These results also show that, in addition to a collapse driven by the overpressure that develops at the base of a wall that is not able to drain efficiently, a second mechanism is possible that can affect even a well maintained wall that is otherwise draining effectively. In this case, failure is driven by a matric suction dissipation under conditions of an extreme rainfall event of a high return period (100 years) preceded by 15 days of abundant precipitation. This combination of events has a low probability of occurrence so this failure mechanism has not yet been observed; its occurrence should be confirmed in the future.

ACKNOWLEDGMENTS: We would like to thank the Comunità Montana Valtellina di Tirano and in particular Giovanni Di Trapani and Alessandro Gervasini for their support during many phases of the work, as well as Alessio Conforto. Thanks also to geologist Maurizio Azzola, who kindly answer every question about the events of 1983, and shared his material with us. The Authors would also like to thank the anonymous reviewers for their valuable comments and suggestions that helped to improve the original version of the manuscript.

# REFERENCES

Agostoni S Laffi R, Sciesa E (1997): Centri abitati instabili della provincia di Sondrio. CNR-GNDCI, Milano, 59 pp. + Annexes

Apip, Takara K, Yamashiki Y, Sassa K, Ibrahim AB, Fukuoka H (2010) A distributed hydrological-geotechnical model using satellite-derived rainfall estimates for shallow landslide prediction system at a catchment system. Landslides 7:237-258, DOI 10.1007/s10346-010-0214-z

ASTM (2010) Standard Practice for Classification of Soils for Engineering Purposes (Unified Soil Classification System) – American Society for Testing Materials D2487 – 10

ASTM (2007) Standard Test Method for Density and Unit Weight of Soil in Place by the Sand-Cone Method - American Society for Testing and Materials D1556 – 07

ASTM (2006) Standard Test Method for Permeability of Granular Soils (Constant Head) - American Society for Testing and Materials D2434 – 06

ASTM (2004) Standard Test Method for Direct Shear Test of Soils Under Consolidated Drained Conditions - American Society for Testing and Materials D3080 – 04

Azzola M, Tuia T (1983) Osservazione sui fenomeni franosi che hanno interessato i vigneti terrazzati a monte di Tresenda nel maggio 1983. Geologia Tecnica, Ed. Ordine Nazionale dei Geologi, Rome, Italy 4:23-35

Bacchini M, Zannoni A (2003) Relations between rainfall and triggering of debris-flow: case study of Cancia (Dolomites, Northeastern Italy). Nat Hazards Earth Syst Sci 3:71-79

Beltrami G, Bianchi A, Bonsignore G, Callegari E, Casati P, Crespi R, Dieni I, Gnaccolini M, Liborio G, Montrasio A, Mottana A, Ragni U, Schiavinato G, Zanettin B (1971) Carta Geologica d'Italia alla scala 1:100.000. Foglio 19 Tirano - Servizio Geologico d'Italia

Blahut J, Poretti I, De Amicis M, Sterlacchini S (2012) Database of geo-hydrological disasters for civil protection purposes. Nat Hazards 60(3):1065–1083, DOI 10.1007/s11069-011-9893-6

Caine N (1980) The rainfall intensity-duration control of shallow landslides and debris flows. Geografiska Annaler 62A:23-27

Camera C, Masetti M, Apuani T (2012) Rainfall, infiltration, and groundwater flow in a terraced slope of Valtellina (Northern Italy): Field data and modelling. Environ Earth Sci 65(4):1191-1202, DOI 10.1007/s12665-011-1367-3

Cancelli A, Nova R (1985) Landslides in soil debris cover triggered by raistorms in Valtellina (Central Alps – Italy). In: Proceedings of the IV international conference and field workshop on landslides, Tokio, August 1985, pp 267–272

Ceriani M, Lauzi S, Padovan N (1992) Rainfalls and landslides in the alpine area of Lombardia Region – Central Alps – Italy. In: Internationales Symposion Interpraevent. Bern (Switzerland), 1992, Band 2, pp 9-20

Choi J, Oh HJ, Won JS, Lee S (2010) Validation of an artificial neural network model for landslide susceptibility mapping. Environ Earth Sci 60:473-483, DOI 10.1007/s12665-009-0188-0

Corominas J, Moya J (1999) Reconstructing recent landslide activity in relation to rainfall in the Llobregat River basin, Eastern Pyrenees, Spain. Geomorphology 30:79-93, DOI 10.1016/S0169-555X(99)00046-X

Crosta GB (1990) A study of slope movements caused by heavy rainfall in Valtellina (July 1987). In: Proc. 6th International Conference and Field Workshop on Landslides, Milan, pp 247–258

Crosta GB, Frattini P (2001) "Rainfall tresholds for triggering soil slips and debris flow. In: Proceedings of EGS 2nd Plinius Conference 2000, Mediterranean Storms, Siena, pp 463-488

Crosta GB, Dal Negro P, Frattini P (2003) Soil slips and debris flows on terraced slopes. Nat Hazards Earth Syst Sci 3:31-43

Crozier MJ (1999) Prediction of rainfall-triggered landslides: a test of the antecedent water status model. Earth Surf Process Land 24:825-833, DOI: 10.1002/(SICI)1096-9837(199908)24

Dahal RK, Hasegawa S, Nonomura A, Yamanaka M, Masuda T, Nishino K (2008) GIS-based weights of evidence modelling of rainfall-induced landslides in small catchments for landslide susceptibility mapping. Environ Geo 54:311-324, DOI 10.1016/j.geomorph.2008.05.041

Fleming RW, Ellen SD, Algus MA (1989) Transformation of dilative and contractive landslide debris into debris flows—an example from Marin County, California. Eng Geol 27:201–223, DOI 10.1016/0013-7952(89)90034-3

Fredlund DG, Rahardjo H (1993) Soil Mechanics for Unsaturated Soils. Wiley, New York.

GEO-SLOPE International Ltd. (2002a) SEEP/W User's Guide, Version 5, Calgary

GEO-SLOPE International Ltd. (2002b) SIGMA/W User's Guide, Version 5, Calgary

Gosso G, Spalla MI, Bini A, Siletto GB, Berra F, Forcella F, Cariboni M, Corbari D, Ferliga C, Gazzola D, Rodeghiero F, Tognini P (in press) Carta Geologica d'Italia alla scala 1:50.000. Foglio 057 Malonno – Istituto Superiore per la Protezione e la Ricerca Ambientale, Servizio Geologico d'Italia

Govi M, Mortara G, Sorzana PF (1985) Eventi idrologici e frane. Geol Appl e Idrog 20(2): 359–375

Guzzetti F, Crosta G, Marchetti M, Reichenbach P (1992) Debris flows triggered by the July, 17–19, 1987 storm in the Valtellina area (Northern Italy). In: International Symposium Interpraevent 1992, Bern, Switzerland, pp 193-203

Guzzetti F, Perruccacci S, Rossi M, Stark CP (2008) The rainfall intensity-duration control of shallow landslides and debris flows: an update. Landslides 5:3-17, DOI 10.1007/s10346-007-0112-1

Harkness RM, Powrie W, Zhang X, Brady KC, O'Reilly MP (2000) Numerical modeling of full-scale tests on drystone masonry retaining walls. Geotechnique 50(2):165-179, DOI 10.1680/geot.2000.50.2.165

Hungr O, Evans SG, Bovis MJ, Hutchinson JN (2001) A review of the classification of landslides of the flow type. Environmental and Engineering Geoscience 7(3):221-238

Hungr O, Leroueil S, Picarelli L (2012) Varnes classification of landslide types, an update. In Landslides and Engineered Slopes. Protecting Society through Improved Understanding. E Eberhardt, C Froeses, A Keith Turner & S Leroueil. Eds CRC Press. Vol 1: 47-58

Ibsen ML, Casagli N (2004) Rainfall patterns and related landslide incidence in the Porretta-Vergato region, Italy. Landslides 1:143-150, DOI 10.1007/s10346-004-0018-0

Itasca Consulting Group Inc. (2008) FLAC Version 6.00. User's Guide, Fourth Edition, Minneapolis

Iverson RM, Reid ME, LaHusen R (1997) Debris-flow mobilization from landslides. Annu Rev Earth Planet Sci 25:85-138.

Jacob M, Holm K, Lange O, Schwab JW (2006) Hydrometeorological thresholds for landslide initiation and forest operation shutdowns on the north coast of British Columbia. Landslides 3(3):228–238, DOI 10.1007/s10346-006-0044-1

Jakob M, Lambert S (2009) Climate change effects on landslides along the southwest coast of British Columbia. Geomorphology 107:275-284, DOI 10.1016/j.geomorph.2008.12.009

Johnson AM, Rahn PH (1970) Mobilization of debris flows. In: Macar P (ed) New Contributions to Slope Evolution. Zeitschrift für Geomorphologie Neue Folge. Supplementband, vol 9, pp 168–186

Khan YA, Lateh H, Baten MA, Kamil AA (2011) Critical antecedent rainfall conditions for shallow landslides in Chittagong City of Bangladesh. Environ Earth Sci. DOI 10.1007/s12665-011-1483-0

Kuriakose SL, van Beek LPH, van Westen CJ (2009) Parameterizing a physically based shallow landslide model in a data poor region. Earth Surf Process Land 34:867-881, DOI 10.1002/esp.1794

Lee S, Pradhan B (2007) Landslide hazard mapping at Selangor, Malaysia using frequency ratio and logistic regression models. Landslides 4:22-41, DOI 10.1007/s10346-006-0047-y

Lourenço PB, Oliveira DV, Roca P, Orduña A (2005) Dry joint stone masonry walls subjected to In-Plane combined loading. J Struct Eng 131(11):1665-1673, DOI: 10.1061/(ASCE)0733-9445(2005)131:11(1665)

Luino F, Nigrelli G, Biddoccu M, Cirio CG, Di Palma M, Missaglia M, Fassi P (2008) Definizione delle soglie pluviometriche d´innesco di frane superficiali e colate torrentizie: accorpamento per aree omogenee. IRER, Milano

Montrasio L, Valentino R, Losi GL (2009) Rainfall-induced shallow landslides: a model for the triggering mechanism of some case studies in Northern Italy. Landslides 6:241-251, DOI 10.1007/s10346-009-0154-7

Powrie W, Harkness RM, Zhang X, Bush DI (2002) Deformation and failure modes of drystone retaining walls. Geotechnique 52(6):435-446, DOI 10.1680/geot.2002.52.6.435

Pradhan B, Lee S (2010) Regional landslide susceptibility analysis using back-propagation neural network model at Cameron Highland, Malaysia. Landslides 7:13-30, DOI 10.1007/s10346-009-0183-2

Quan Luna B, van Westen CJ, Blahut J, Camera C, Apuani T, Sterlacchini S (2010) From deterministic hazard modelling to risk and loss estimation. In: Mountain Risks: Bringing Science to Society. Proceedings of the International Conference, 24-26th November 2010, Florence, Italy. CERG Editions, Strasbourg, pp 373-380

Rahardjo H, Li XW, Toll DG, Leong EC (2001) The effect of antecedent rainfall on slope stability. Geotech Geol Eng 19:371-399, DOI: 10.1023/A:1013129725263

Revellino P, Guadagno FM, Hungr O (2008) Morphological methods and dynamic modeling in landslide hazard assessment of the Campania Apennine carbonate slope. Landslides 5:59–70. DOI 10.1007/s10346-007-0103-2

Salciarini D, Godt JW, Savage WZ, Conversini P, Baum RL, Michael JA (2006) Modeling regional initiation of rainfall-induced shallow landslides in the eastern Umbria Region of central Italy. Landslides 3:181–194, DOI 10.1007/s10346-006-0037-0

Simoni S, Zanotti F, Bertoldi G, Rigon R (2008) Modelling the probability of occurrence of shallow landslides and channelized debris flows using GEOtop-FS. Hydrol Process 22 :532–545, DOI: 10.1002/hyp.6886

Tsai TL (2008) The influence of rainstorm pattern on shallow landslide. Environ Geol 53:1563-1569, DOI 10.1007/s00254-007-0767-x

Tsai TL, Chen HE, Yang JC (2008) Numerical modeling of rainstorm-induced shallow landslides in saturated and unsaturated soils. Environ Geol 55:1269-1277, DOI 10.1007/s00254-007-1075-1

van Beek LPH, van Asch TWJ (2004) Regional assessment of the effects of land-use change on landslide hazard by means of physically based modelling. Nat Hazards 31:289-304

Villemus B, Morel JC, Boutin C (2007) Experimental assessment of dry retaining wall stability on a rigid foundation. Eng Struct 29:2124-2132, DOI 10.1016/j.engstruct.2006.11.007

Walker P, McCombie P, Claxton M (2007) Plane strain numerical model for drystone retaining walls. Geotech Eng 160( GE2):97-103, DOI: 10.1680/geng.2007.160.2.97

Zezere JL, Trigo RM, Trigo IF (2005) Shallow and deep landslides induced by rainfall in the Lisbon region (Portugal): assessment of relationships with the North Atlantic Oscillation. Nat Hazard Earth Syst Sci 5:331-344, DOI 10.5194/nhess-5-331-2005

Zhang X, Koutsabeloulis NC, Hope S, Pearce A (2004) A finite element analysis for the stability of drystone masonry retaining walls. Geotechnique 54(1):57-60

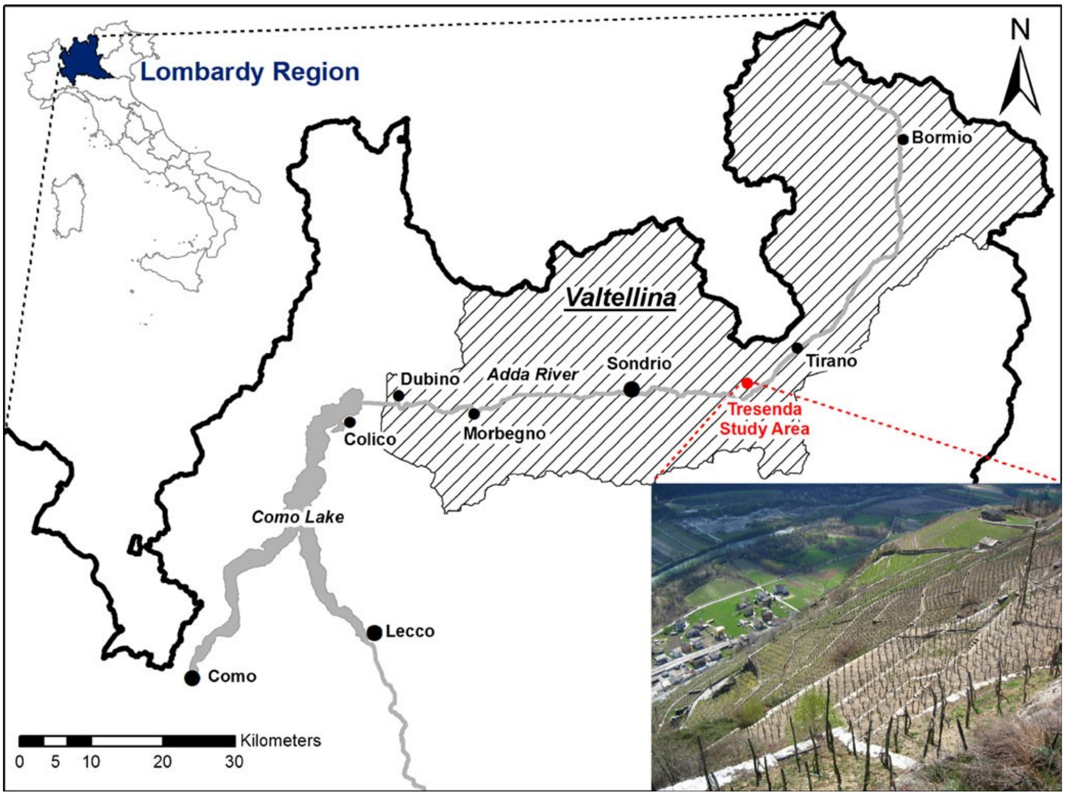


*Fig. 1 Geographical setting of the study area*

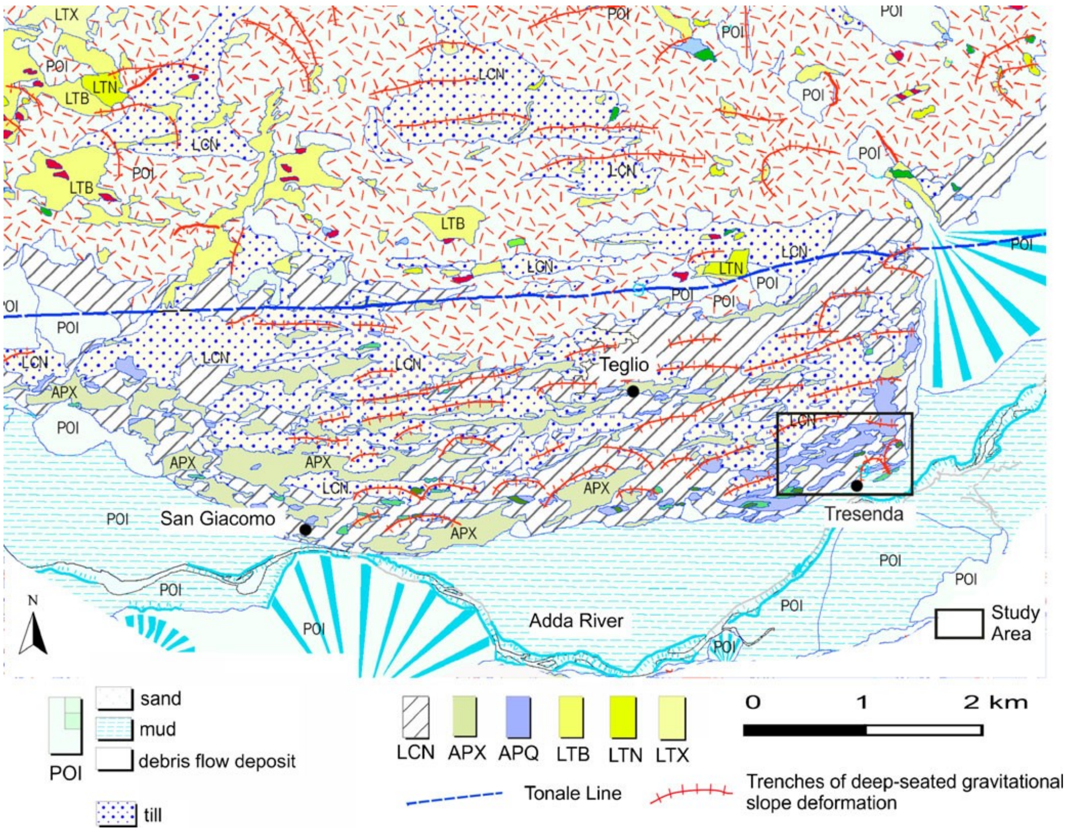


*Fig. 2 Simplified geological map of the study area and surrounding area (modified after Gosso et al. 2012) Neogene to Quaternary continental deposits: Po Syntheme (POI); Cantù Syntheme (LCN); Austroalpine metamorphic basement–Languard-Tonale tectonometamorphic unit: two mica- or biotite- metasedimentary gneisses (LTB); sillimanite, biotite, and garnet metasedimentary gneisses (LTN); garnet–staurolite micaschists (LTX); Variscan metamorphic basement of the southern Alps – Aprica tectonometamorphic units: garnet, biotite, and chlorite micaschists (APX), Quartzites (APQ)*

*Fig. 3 Two photos of the soil slip/debris avalanche events that in May 1983 affected the slope of Tresenda. Top: a panoramic of the slope; bottom: a detail of the source area of the event on the left in the top image. Photos by Maurizio Azzola*

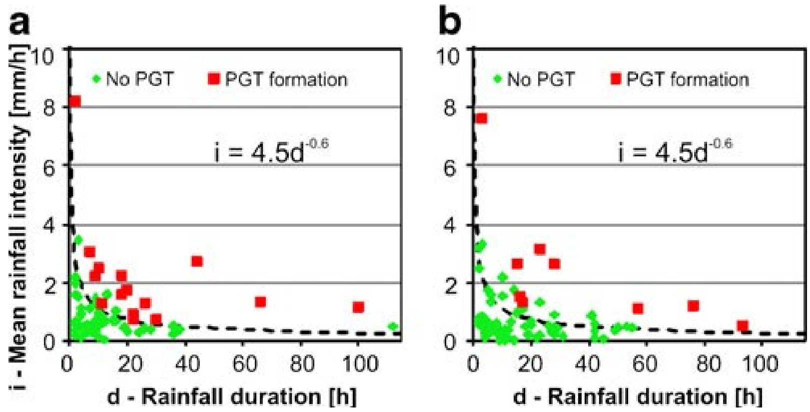


*Fig. 4 Rainfall intensity–duration threshold for PGT formation.* ***a*** *The threshold drawn from the data of the period August 2009 to August 2010 as presented in Camera et al. (2012).* ***b*** *Validation of the threshold performed with the data from August 2010 to August 2011*

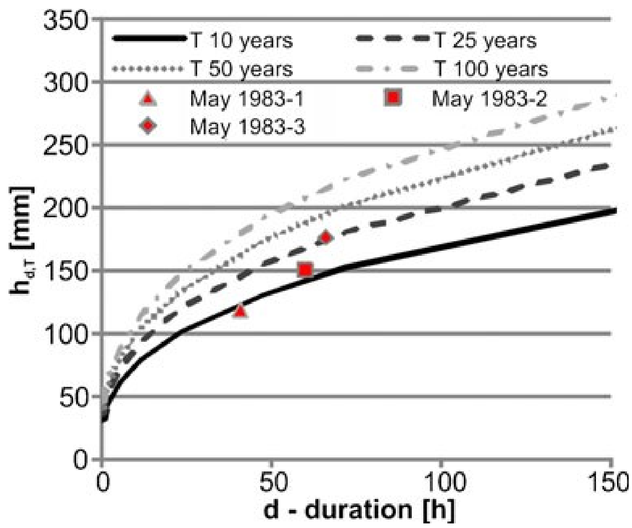


*Fig. 5 Rainfall intensity–duration frequency curves for return periods (T) of 10, 25, 50, and 100 years. The three points on the graph depict the landslide triggering rainfall event of 1983 by associating the recurrence time to three pairs of cumulated duration–height recorded before the triggering of the three debris avalanches occurred on the 22nd and 23rd of May 1983*

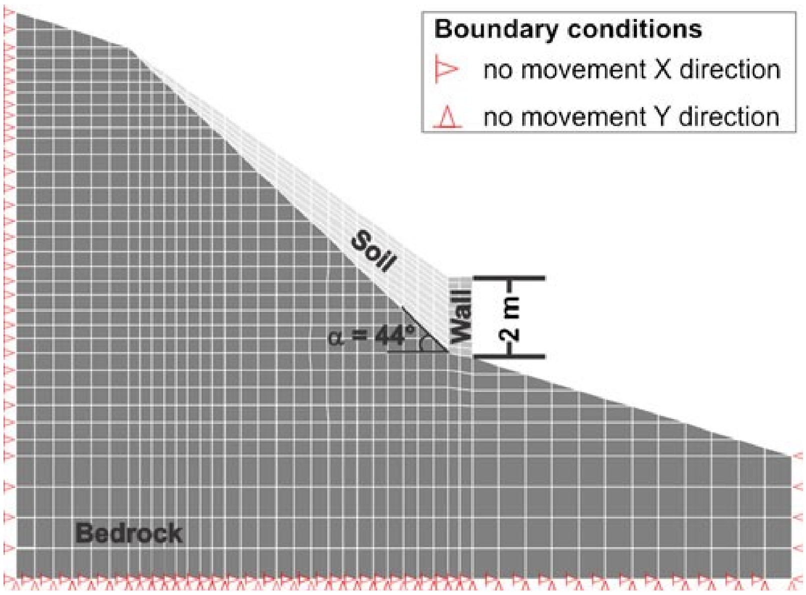


*Fig. 6 Model geometry and boundary conditions*

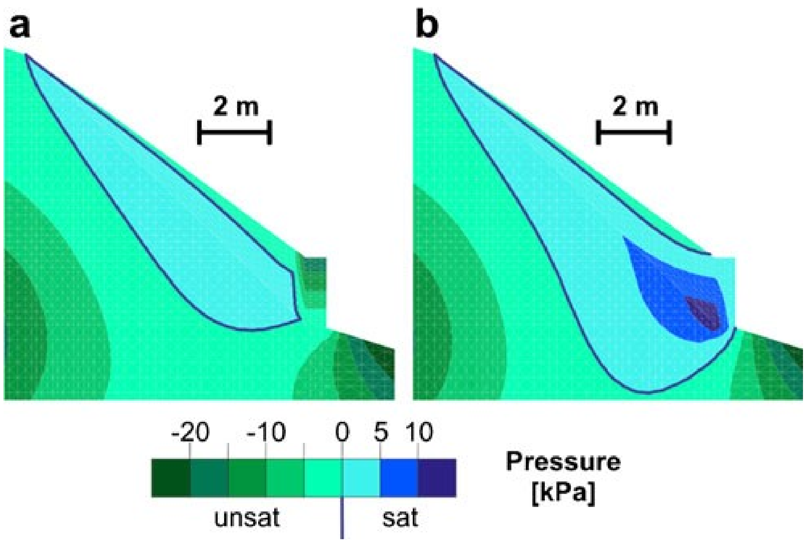


*Fig. 7 Overpressures developed at the wall base (kilopascal) for the project rainfall event of 72 h and 50-year return period, with a well-maintained wall* ***(a)*** *and an old, poorly maintained structure* ***(b)****. Results obtained from SEEP/W*

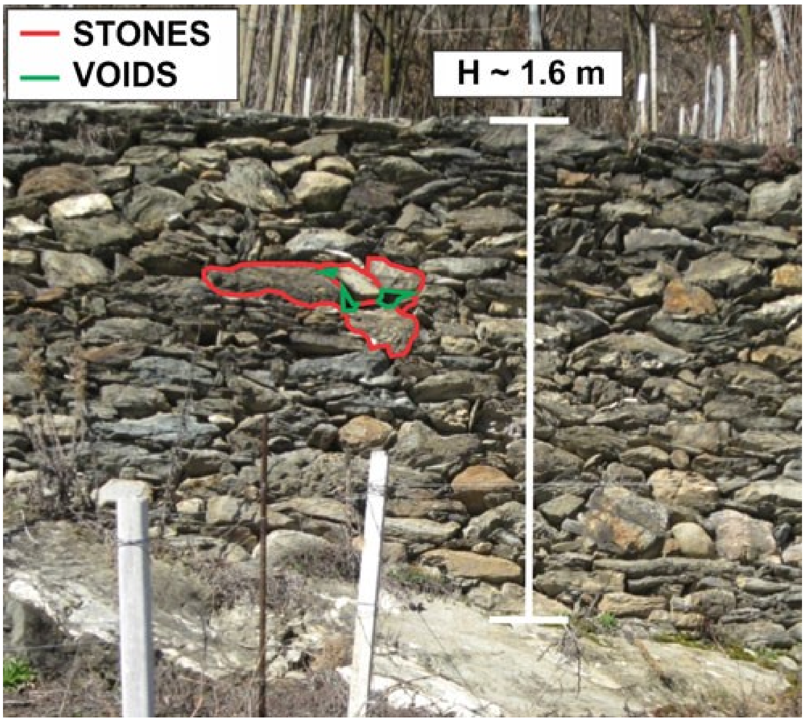


*Fig. 8 A dry stone wall with the stones and voids structure*

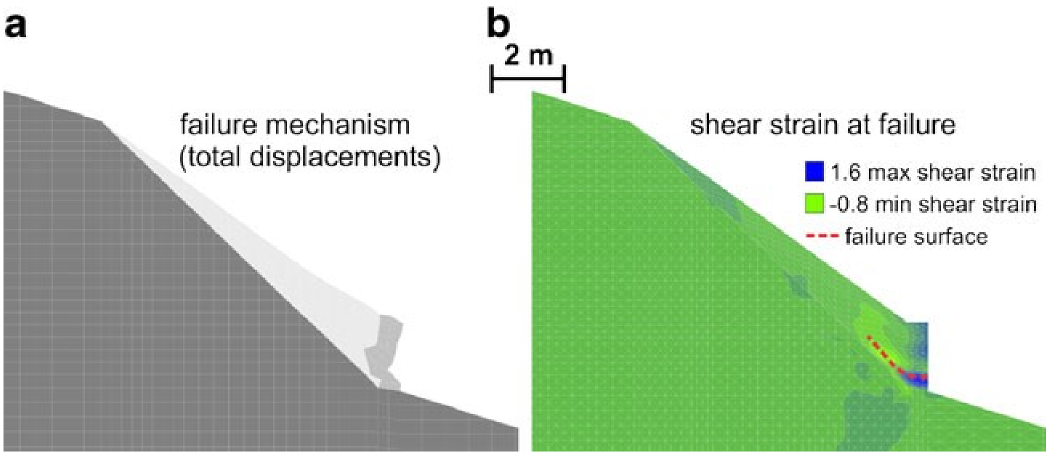


*Fig. 9* ***a*** *Time of failure represented by the displacements experienced by the wall;* ***b*** *XY shear strain [−] developed in the model. Results obtained from SIGMA/W*

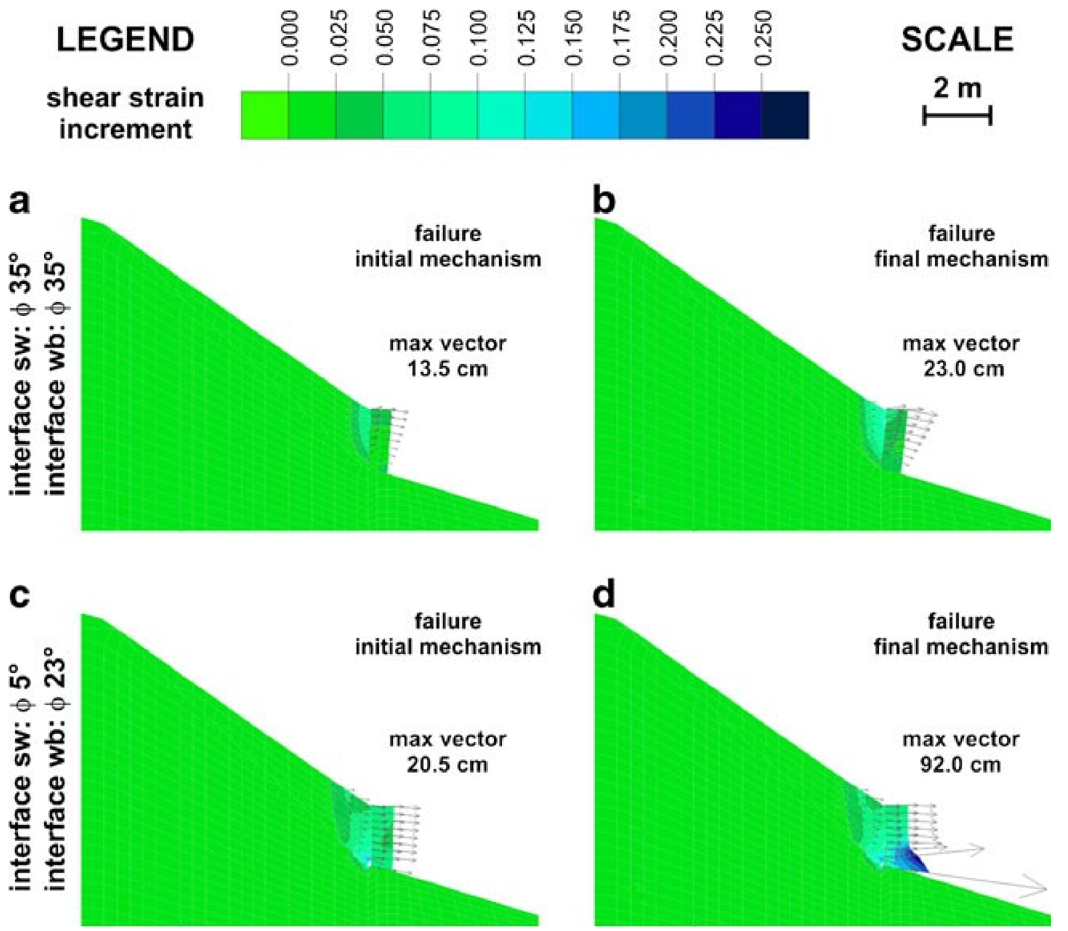


*Fig. 10 Results obtained from FLAC showing the shear strain increments and the displacement vectors. Initial (**a, c**) and final (**b, d**) failure mechanisms depending from soil–wall (sw) and wall–bedrock (wb) friction angle*

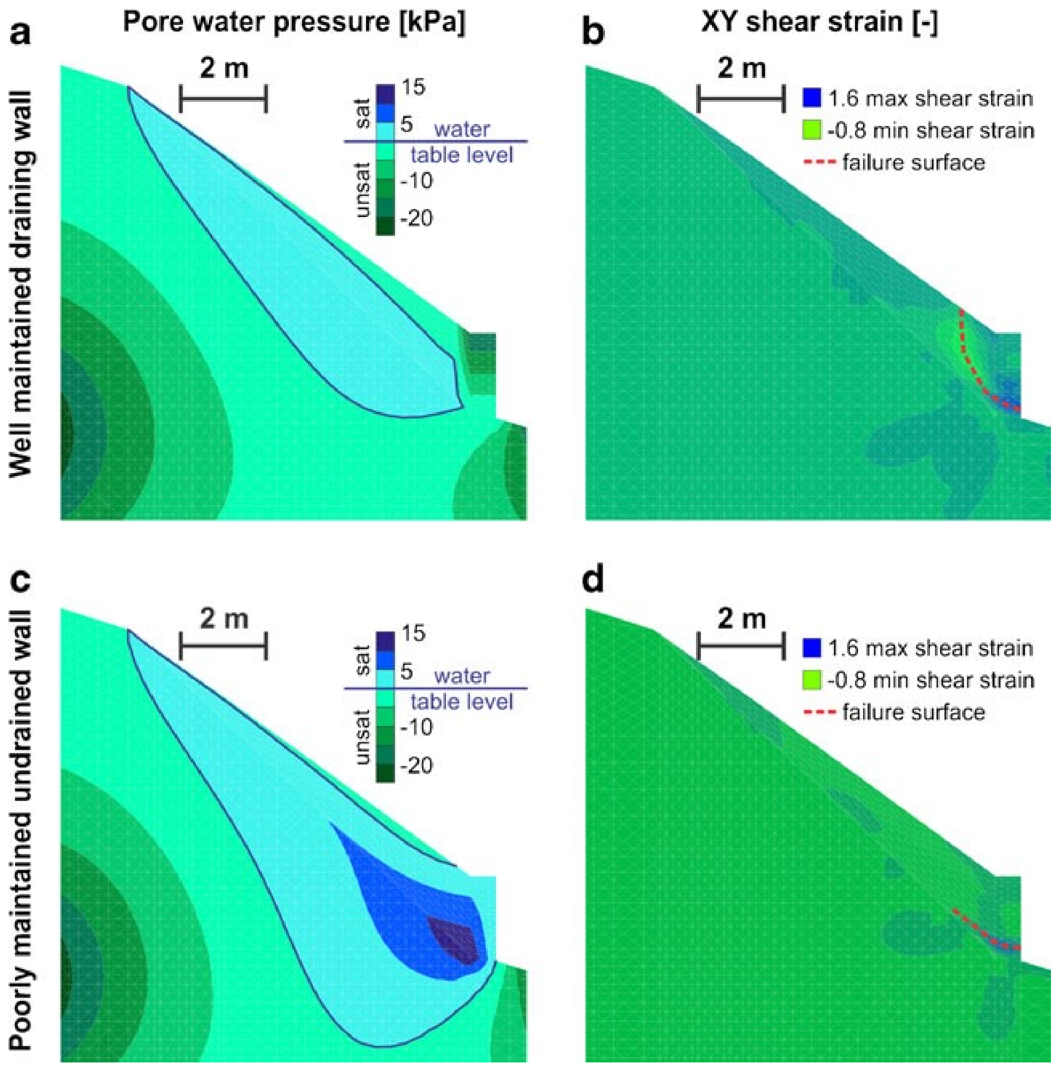


*Fig. 11 Pore water pressure distribution in kilopascal at the moment of collapse for a well-maintained wall (**a**) and a poorly maintained wall (**c**) as calculated from SEEP/W. The corresponding states of XY shear strain, showing different failure surfaces as calculated from SIGMA/W (**b, d**)*

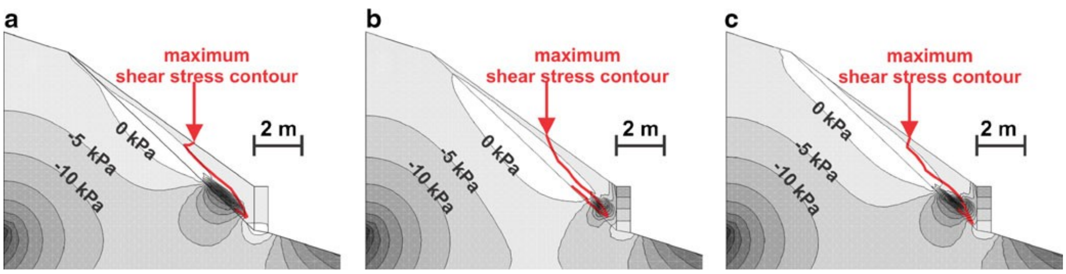


*Fig. 12 Contours represent the pore pressure distribution at the time step immediately prior to the collapse for three different combinations of cohesion and friction angle values for the wall. The simulations refer to the calibration phase performed with the FE model. **a** $c_0$ 30 kPa, $\phi_0$ 50°; **b** $c_0$ 40 kPa, $\phi_0$ 50°; **c** $c_0$ 90 kPa, $\phi_0$ 55°. The contour of the maximum shear stress tends to develop at the contact between the saturated and unsaturated soil*

Table 2 Summary of the hydrogeological and geotechnical principal properties of the backfill soils: saturated hydraulic conductivity ($k_s$) obtained with different methods: double ring (DR) and hole (H) infiltrometric tests, falling (FH) and constant head (CH) permeability tests; dry and natural bulk weight ($\gamma_d$ and $\gamma_0$, respectively); peak values of cohesion ($c_p$) and friction angle ($\phi_p$); residual values of cohesion ($c_r$) and friction angle ($\phi_r$).

| Parameter | Min | Mean | Max |
|---|---|---|---|
| $k_{s(DR)}$ [m/s] | $2.0 \times 10^{-6}$ | $3.2 \times 10^{-5}$ | $5.5 \times 10^{-5}$ |
| $k_{s(H)}$ [m/s] | $1.4 \times 10^{-6}$ | $3.8 \times 10^{-5}$ | $1.2 \times 10^{-4}$ |
| $k_{s(FH)}$ [m/s] | $3.2 \times 10^{-6}$ | $5.3 \times 10^{-6}$ | $1.5 \times 10^{-5}$ |
| $k_{s(CH)}$ [m/s] | $2.1 \times 10^{-6}$ | $4.7 \times 10^{-6}$ | $9.9 \times 10^{-6}$ |
| $\gamma_d$ [kN/m$^3$] | 12.8 | 13.8 | 15.7 |
| $\gamma_0$ [kN/m$^3$] | 13.8 | 14.9 | 16.1 |
| $c_p$ [kPa] | 3.4 | 10.7 | 18.5 |
| $\phi_p$ [°] | 27.5 | 33.8 | 36.5 |
| $c_r$ [kPa] | 6.6 | 12.9 | 17.0 |
| $\phi_r$ [°] | 26.3 | 30.4 | 36.5 |

Table 2 Summary of the results obtained using the calibrated stability model. During the different simulations return period of input rainfalls, walls maintenance conditions and initial volumetric water content of soil were varied.

| ID | Return period | Wall | Initial condition | Result FEM | Result FDM |
|---|---|---|---|---|---|
| 1 | 10 years | Well-maintained | Dry | Stable | Stable |
| 2 | 10 years | Well-maintained | Wet | Stable | Stable |
| 3 | 10 years | Poorly-maintained | Dry | Stable | Stable |
| 4 | 10 years | Poorly-maintained | Wet | Stable | Stable |
| 5 | 50 years | Well-maintained | Dry | Stable | Stable |
| 6 | 50 years | Well-maintained | Wet | Stable | Stable |
| 7 | 50 years | Poorly-maintained | Dry | Stable | Stable |
| 8 | 50 years | Poorly-maintained | Wet | Stable | Unstable |
| 9 | 100 years | Well-maintained | Dry | Stable | Stable |
| 10 | 100 years | Well-maintained | Wet | Unstable | Stable |
| 11 | 100 years | Poorly-maintained | Dry | Stable | Stable |
| 12 | 100 years | Poorly-maintained | Wet | Unstable | Unstable |